batteries

Article

Preparation of Mesoporous Boron-Doped Porous Carbon Derived from Coffee Grounds via Hybrid Activation for Carbon Capture and Storage

Hyeon Hye Kim [1,2], Kay-Hyeok An [3,*] and Byung-Joo Kim [1,3,*]

[1] Material Application Research Institute, Jeonju University, Jeonju 55069, Republic of Korea; hyeon_h@jj.ac.kr
[2] School of Polymer Science and Engineering, Chonnam National University, Gwangju 61186, Republic of Korea
[3] Department of Materials Science and Chemical Engineering, Jeonju University, Jeonju 55069, Republic of Korea
* Correspondence: khandragon@jj.ac.kr (K.-H.A.); kimbyungjoo@jj.ac.kr (B.-J.K.)

Abstract: The increasing concentration of carbon dioxide (CO_2) in the atmosphere necessitates the development of efficient carbon capture and storage (CCS) technologies. Among these, adsorption-based methods using porous carbon (PC) have attracted considerable attention due to their low energy requirements and cost-effectiveness. Biomass waste-derived porous carbon is particularly attractive as a sustainable alternative, offering environmental benefits and high-value applications with low costs. In this study, coffee grounds (CGs) were selected as a precursor due to their abundance and cost-effectiveness compared with other biomass wastes. To improve the pore characteristics of CG-derived carbon (CCG), boric acid treatment was applied during carbonization followed by steam activation to prepare boron-doped CG-derived porous carbon (B-PCG). The N_2/77K adsorption–desorption isotherms revealed a significant increase in the specific surface area and total pore volume of B-PCG from 1590 m^2/g and 0.71 cm^3/g to 2060 m^2/g and 1.01 cm^3/g, respectively, compared with PCG. Furthermore, high pressure CO_2 adsorption analysis at 298 K up to 50 bar showed an approximately 50% improvement in CO_2 adsorption capacity for B-PCG compared with PCG. These results suggest that boron doping is an effective strategy to optimize the pore structure and adsorption performance of biomass-derived porous carbon materials for CCS application.

Keywords: carbon capture and storage; porous carbon; coffee grounds; low cost; boron

Academic Editors: Binghui Xu and Haichao Chen

Received: 14 March 2025
Revised: 13 April 2025
Accepted: 15 April 2025
Published: 17 April 2025

Citation: Kim, H.H.; An, K.-H.; Kim, B.-J. Preparation of Mesoporous Boron-Doped Porous Carbon Derived from Coffee Grounds via Hybrid Activation for Carbon Capture and Storage. *Batteries* **2025**, *11*, 158. https://doi.org/10.3390/batteries11040158

1. Introduction

Globally, anthropogenic activities related to energy production and consumption are among the major contributors to global warming. In particular, the increasing concentration of greenhouse gases (GHGs) in the atmosphere has intensified the frequency and magnitude of climate change phenomena, including abnormal temperatures, rising sea levels, and extreme weather events [1–3]. Addressing global warming has thus emerged as a critical challenge for the international community and the global scientific community. In response, the European Commission has established an energy roadmap to achieve climate neutrality by 2050, emphasizing the importance of renewable energy sources in decarbonizing the energy sector [4,5]. Currently, fossil fuels such as coal, oil, and natural gas account for approximately 82% of the global energy consumption. However, their combustion significantly increases GHG emissions, making them a major cause of environmental issues. Consequently, carbon capture and storage (CCS) technology has gained

increasing attention as a sustainable approach to drastically reduce the concentration of excessive GHGs, such as CO_2, emitted from large-scale energy production systems [6,7].

Considering the depletion of fossil-based resources and their significant impact on environmental pollution, the development of sustainable and environmentally friendly alternative resources is imperative. In this context, the use of waste biomass offers significant environmental and economic benefits [8,9]. Agricultural biomass waste, including crop stalks, leaves, roots, coffee cherries, fruit peels, seeds, and nutshells, is typically disposed of in landfills or incinerated, which can have detrimental environmental effects [10]. Biomass waste is rich in cellulose, hemicellulose, and lignin, making it applicable to various industrial sectors such as fuel production, polymer manufacturing, and construction materials [11–13]. However, the high-value utilization of biomass wastes remains limited, except for certain materials such as rice husks, sugarcane bagasse, and wheat straw [14]. Moreover, only a small fraction of biomass waste is used as feedstock for industrial applications and power production generation, while the majority is either left untreated or incinerated, resulting in groundwater, air, and soil contamination, increased pest infestation, and adverse effects on human health. Notably, the decomposition of unregulated biomass waste in soils can release nitrogen oxides (NO and N_2O), which have a significantly higher global warming potential than CO_2 [15,16]. Worldwide, over 2 gigatons (Gt) of agricultural waste are incinerated annually, contributing approximately 18% of global CO_2 emissions and releasing substantial amounts of particulate matter and black carbon [17].

Coffee is one of the most popular beverages in modern society, with an annual production exceeding 5 million tons [18]. Over the past three decades, the global demand for coffee has steadily increased, leading to the expansion of coffee production and exports worldwide. As a result, global coffee production has risen by more than 60%. Consequently, the quantity of biomass waste in the form of coffee grounds (CGs) has also increased, with over 10.5 million tons generated annually [19]. Typically, CGs are disposed of in landfills or by incineration, with the latter process emitting approximately 338 kg of CO_2 per ton of CGs burned. Additionally, methane gas generated during landfilling has a greenhouse effect approximately 25 times greater than that of CO_2, underscoring the urgent need for efficient CG utilization strategies [20,21].

Reuse and recycling of agricultural biomass wastes offer potential benefits for carbon neutrality but also pose complex challenges, including land use changes, soil nutrient depletion, and environmental and health concerns [22]. To address these issues, research efforts have focused on converting low-cost biomass wastes into environmentally friendly and high-value materials. In developed countries, initiatives to minimize biomass waste disposal and promote its use in energy and heat production have been increasing. For instance, in Europe, open burning of agricultural waste has been prohibited, and wheat straw has become a primary feedstock for bioenergy production. Many countries are striving to recover and utilize biomass waste as a resource while avoiding incineration and landfilling [23–25]. However, the increased utilization of biomass waste requires specific management strategies to address the challenges associated with the significant amount of ash produced during combustion and pyrolysis processes [26].

This study aims to address the growing problem of biomass waste and maximize the potential of carbon-based materials by recycling CGs into high-value porous carbon materials. CGs are particularly advantageous as a precursor for porous carbon synthesis due to their abundant supply and low raw material cost [27–29]. Additionally, during the coffee extraction process, intrinsic molecules such as caffeine, tannins, and polyphenols are leached out, naturally creating multiple voids. These internal voids can be transformed into a hierarchical porous structure through thermal treatment, and surface modifications can introduce various functional groups, enhancing their potential for energy storage applications [30,31].

Furthermore, CG-derived porous carbon materials exhibit excellent adsorption properties, making them suitable for water purification and gas adsorption applications. Previous studies have reported that coffee by-products can be converted into high-performance adsorbents via carbonization and chemical modification processes, demonstrating their effectiveness in pollutant removal [32]. The development of CG-derived porous carbon materials holds significant promise for various applications, including electrode materials for energy storage devices and adsorbents for environmental remediation [33–35]. In particular, this study focuses on optimizing the structural properties of CG-based porous carbon materials through activation processes and enhancing CO_2 selectivity by heteroatom doping as a surface modification strategy. In general, porous carbon materials possess well-developed pore structures, large surface areas, excellent electrical conductivity, and remarkable chemical stability. These properties make them promising candidates for gas adsorption applications, and their performance can be significantly enhanced by surface treatments. However, conventional porous carbons typically suffer from hydrophobic surfaces and a limited number of specific active sites, which restrict their effectiveness in particulate CO_2 capture applications [36,37].

To address these limitations, considerable research has been devoted to the heteroatom doping of carbon materials with elements such as B, N, O, and P, which can improve their electrochemical properties, CO_2 adsorption capacity, and selectivity [38–40]. Among these, B is particularly effective, as it can substitute carbon atoms within the lattice, acting as an electron acceptor due to its three valence electrons. This substitution modifies the electronic structure of the doped carbon by shifting the Fermi level toward the conduction band. B-containing functional groups incorporated on the CG surface are expected to enhance CO_2 capture performance by providing additional active sites for efficient CO_2 molecules.

Therefore, this study proposes the synthesis of boron-doped porous carbon using CGs as a precursor and its application in CCS. This approach aims to provide a high-value utilization pathway for biomass waste while contributing to greenhouse gas reduction and sustainable environmental protection.

2. Materials and Methods

2.1. Materials and Preparation of Boric Acid-Treated Coffee Grounds

The CGs used in this study were purchased from Mega Coffee (Seoul, Republic of Korea). To remove residual moisture, the CGs were dried in an oven at 100 °C for 12 h. To remove impurities, 200 g of CGs were immersed in 1500 mL of 1 M hydrogen chloride (HCl) solution at room temperature for 1 h. The samples were then thoroughly washed with distilled water until the pH reached 7.0 and then dried in an oven at 100 °C for 24 h. For dry boric acid pretreatment, 15 g of dried CGs were mixed with 5 g of boric acid (Daejung Chemical & Metals Co., Siheung, Republic of Korea) using a mortar and pestle to ensure homogeneity. The prepared samples were designated as 'B-CGs' and 'CGs' according to the presence or absence of boric acid in the mixture.

2.2. Carbonization and Activation of CGs and B-CGs

A uniformly mixed 20 g quantity of CGs and B-CGs was placed in an alumina boat and loaded into a cylindrical alumina tube furnace (diameter: 90 mm, length: 1000 mm). The samples were carbonized at temperatures ranging from 800 to 1000 °C for 1 h under a nitrogen (N_2) atmosphere (99.99%, 500 cc/min) at a heating rate of 5 °C/min. The resulting carbonized CG (CCG) and boric acid-treated CCG (B-CCG) were subjected to vacuum-assisted washing with distilled water to remove residual borates formed during carbonization. Subsequently, the samples were thoroughly dried in an oven for 24 h. After complete drying, 3.0 g of CCG and B-CCG were placed in an alumina boat and loaded into

a cylindrical stainless steel tube furnace (diameter: 80 mm, length: 1200 mm). The samples were heated to 900 °C under an N_2 atmosphere (99.9999%, 200 mL/min) at a heating rate of 10 °C/min. After reaching 900 °C, the N_2 atmosphere was switched to a steam environment (0.5 mL/min water supply), and the activation process was maintained for 60 min. The synthesized porous carbon derived from coffee grounds (PCG) was designated as 'boric acid treatment (B)–porous carbon derived from coffee grounds (PCG)–carbonization temperature (C8, C9, and C10)'.

2.3. Characterization of PCG

The crystalline structure of PCG was analyzed by X-ray diffraction (XRD; MiniFlex, Rigaku, Tokyo, Japan). XRD analysis was performed with Cu-Kα radiation (0.1542 nm) at a scanning rate of 2°/min over a 2θ range of 5–60°. Crystallite size and interplanar spacing were calculated using the Scherrer and Bragg equations, respectively [41].

The textural properties of PCG were characterized using an N_2/77K adsorption–desorption isothermal analyzer (BELSORP Max II, MicrotracBEL, Tokyo, Japan). Prior to measurement, the samples were degassed at 300 °C under a residual pressure of less than 10^{-3} bar for 12 h to ensure the complete removal of adsorbed impurities and gases. The specific surface area of PCG was determined by the Brunauer–Emmett–Teller (BET) method based on the N_2/77K adsorption–desorption isotherm curves [42]. The pore size distribution (PSD) was calculated using the Barrett–Joyner–Halenda (BJH) method and the non-local density functional theory (NLDFT) [43,44]. Additionally, the micropore volume of PCG was estimated from the intercept value of the t-plot.

Elemental composition and surface functional group analysis of PCG were performed by X-ray photoelectron spectroscopy (XPS; Thermo Scientific NEXSA, Watertown, NY, USA). The samples were analyzed under vacuum conditions at pressures below 3×10^{-7} Pa using Al-Kα radiation (1486.6 eV).

3. Results

3.1. Textural Properties of PCG and B-PCG by Carbonization Temperature

The pore formation and adsorption behavior of PCG and B-PCG as a function of carbonization temperature were analyzed using the N_2/77K adsorption–desorption method, as shown in Figure 1. In Figure 1a, all PCG samples exhibited a type I (a) isotherm according to the classification of the International Union of Pure and Applied Chemistry (IUPAC) [45]. Type I (a) isotherms are typically observed when nitrogen adsorption primarily occurs within micropores at low relative pressures ($P/P_0 \leq 0.1$). This indicates that PCG-C8 to PCG-C10 undergo monolayer adsorption predominantly driven by micropore development. In contrast, B-PCG exhibited a transition to a type I (b) isotherm with a larger specific surface area compared with PCG. The type I (b) adsorption isotherm is generally characteristic of porous materials with both micropores and mesopores.

The basal planes of carbon materials are formed through an sp^2 hybridized bond, while the crystallite edges are composed of sp^3 hybridized bonds. In this study, it was confirmed that doping elements, specifically boron (B), can be introduced in various functionalized forms at the crystallite edges of carbon materials via a dry thermal treatment process utilizing differences in elemental bonding energy. In particular, the transformation of the B-PCG adsorption isotherm to a type I (b) profile suggests that various boron functional groups were incorporated at the crystallite edges of B-CCG during carbonization. Additionally, defects were generated in regions of the basal planes where boron was not incorporated, leading to a gradual increase in pore diameter throughout the activation process. Furthermore, in the relative pressure ranges of $(P/P_0) \leq 0.1$ and $(P/P_0) \leq 0.3$, B-PCG-C8 exhibited higher N_2 adsorption behavior compared with B-PCG-C9 and B-PCG-C10. This

can be attributed to the preferential oxidation of amorphous regions and small crystallites within the structure of B-PCG-C8 at the relatively low carbonization temperature of 800 °C. Generally, during the activation process, oxidation of carbon materials preferentially occurs at amorphous regions and crystallite edges [46]. Consequently, the higher proportion of amorphous structures and small crystallites in B-PCG-C8 facilitates more active oxidation, resulting in the dominant development of micropores and mesopores, as well as an increased specific surface area, as summarized in Table 1.

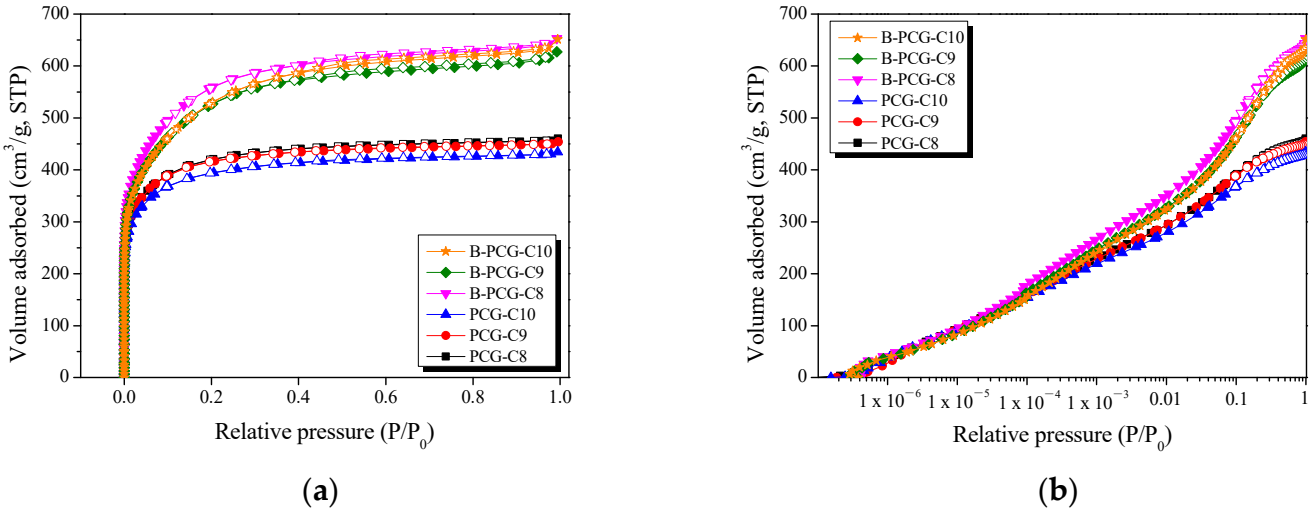

Figure 1. N_2/77K adsorption–desorption isotherm curves of PCG and B-PCG as a function of various carbonization temperatures; (**a**) normal and (**b**) logarithmic.

Table 1. Texture Properties of PCG and B-PCG as a Function of Various Carbonization Temperature.

Sample	S_{BET} [1] (m^2/g)	V_{Total} [2] (cm^3/g)	V_{Micro} [3] (cm^3/g)	V_{meso} [4] (cm^3/g)	Micropore Ratio [5] (%)	Mesopore Ratio [6] (%)
PCG-C8	1590	0.71	0.65	0.06	91.5	8.5
PCG-C9	1580	0.70	0.64	0.06	91.4	8.6
PCG-C10	1490	0.67	0.61	0.06	91.0	9.0
B-PCG-C8	2060	1.01	0.87	0.14	86.1	13.9
B-PCG-C9	1960	0.97	0.82	0.15	84.5	15.5
B-PCG-C10	1940	1.00	0.83	0.17	83.0	17.0

[1] S_{BET}: Specific surface area; Brunauer–Emmett–Teller (BET) method; $\frac{P}{v(P_0-P)} = \frac{1}{v_m} + \frac{c-1}{v_m c} \cdot \frac{P}{P_0}$. [2] V_{Total}: Total pore volume; the amount of adsorbed P/P_0 = 0.99. [3] V_{Micro}: Micropore volume; t-plot method. [4] V_{Meso}: [2] V_{Total} − [3] V_{Micro}. [5] Micropore ratio: $\frac{V_{Micro}}{V_{Total}} \times 100$. [6] Mesopore ratio: $\frac{V_{Meso}}{V_{Total}} \times 100$.

Figure 2a,b indicate the PSD curves of B-PCG obtained by the BJH and NLDFT methods, respectively. In Figure 2a, B-PCG exhibited an increase in mesopores within the 2–5 nm range compared with PCG, regardless of the carbonization temperature. Similarly, in Figure 2b, the PSD curve of B-PCG revealed a greater presence of micropores (1.3–2 nm) along with an increase in mesopores (2–5 nm) compared with PCG. These results are consistent with the N_2/77K adsorption–desorption isotherms in Figure 1, confirming that B-PCG has a more developed pore structure than PCG, not only in the micropore region but also for mesopores smaller than 5 nm.

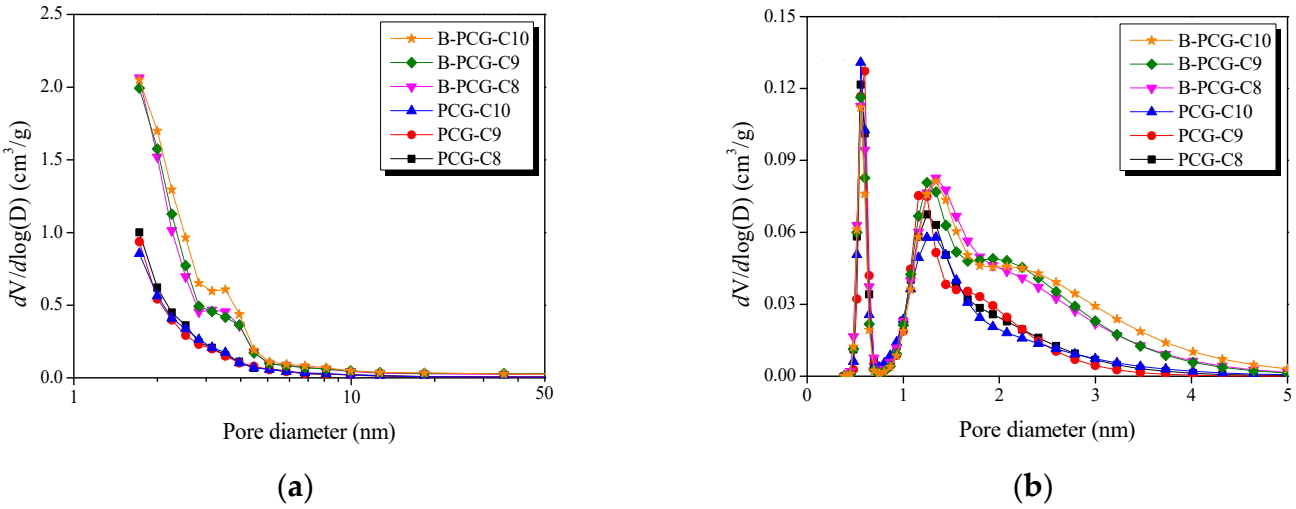

Figure 2. Pore size distribution of PCG and B-PCG as a function of various carbonization temperatures; (**a**) BJH equation and (**b**) NLDFT method.

In general, the mechanism of pore development in porous carbon can be categorized into two processes: (i) pore drilling, where oxidation at crystallite edges increases pore diameter, and (ii) pore deepening, where oxidation of amorphous regions increases pore depth without significant changes in pore diameter [47]. Based on these results, it is inferred that various boron functional groups were incorporated at the crystallite edges of B-PCG. Among them, weakly bonded functional groups such as B–OH and B–H, which are incompletely bonded to carbon, are likely to be decomposed during heat treatment, leading to an increase in pore diameter. In other words, the thermal decomposition of boron functional groups introduced at the crystallite edges of B-PCG promoted pore formation via the pore drilling mechanism. Consequently, boron doping in PCG was found to facilitate the development of both micropores and mesopores, which significantly influenced the formation of a porous structure.

3.2. Crystal Structure of Coffee Grounds Under Various Processing Conditions

To investigate the structural changes in CCG and B-CCG after activation under identical conditions at different carbonization temperatures, XRD pattern analysis was performed, as shown in Figures 3 and 4. As shown in Figure 3a, both CCG and B-CCG exhibited similar trends regardless of carbonization temperature, and no significant structural transformation was observed. For a more quantitative assessment of the structural changes, the crystallite diameter (L_a) and the crystallite height (L_c) were analyzed and are shown in Figure 3b. The results indicate that both the L_a and the L_c increased with increasing carbonization temperature. In particular, the L_a showed a particularly dramatic increase in both CCG and B-CCG. This trend is attributed to the growth of crystallites due to graphitization at higher carbonization temperatures, as well as the influence of boric acid incorporated within the coffee grounds. These effects are further supported by the decrease in interlayer spacing (d_{002}) and the increase in interplanar crystalline spacing (d_{10l}), as shown in Figure 3c. Typically, the d_{002} corresponds to the interlayer spacing between graphitic planes. A decrease in d_{002} suggests that the carbon layers are stacked more closely, which is indicative of an increased degree of graphitization and improved structural ordering. Meanwhile, the increase in the (10*l*) peak intensity reflects enhanced in-plane crystallinity and larger crystallite sizes, further supporting the growth of graphitic domains.

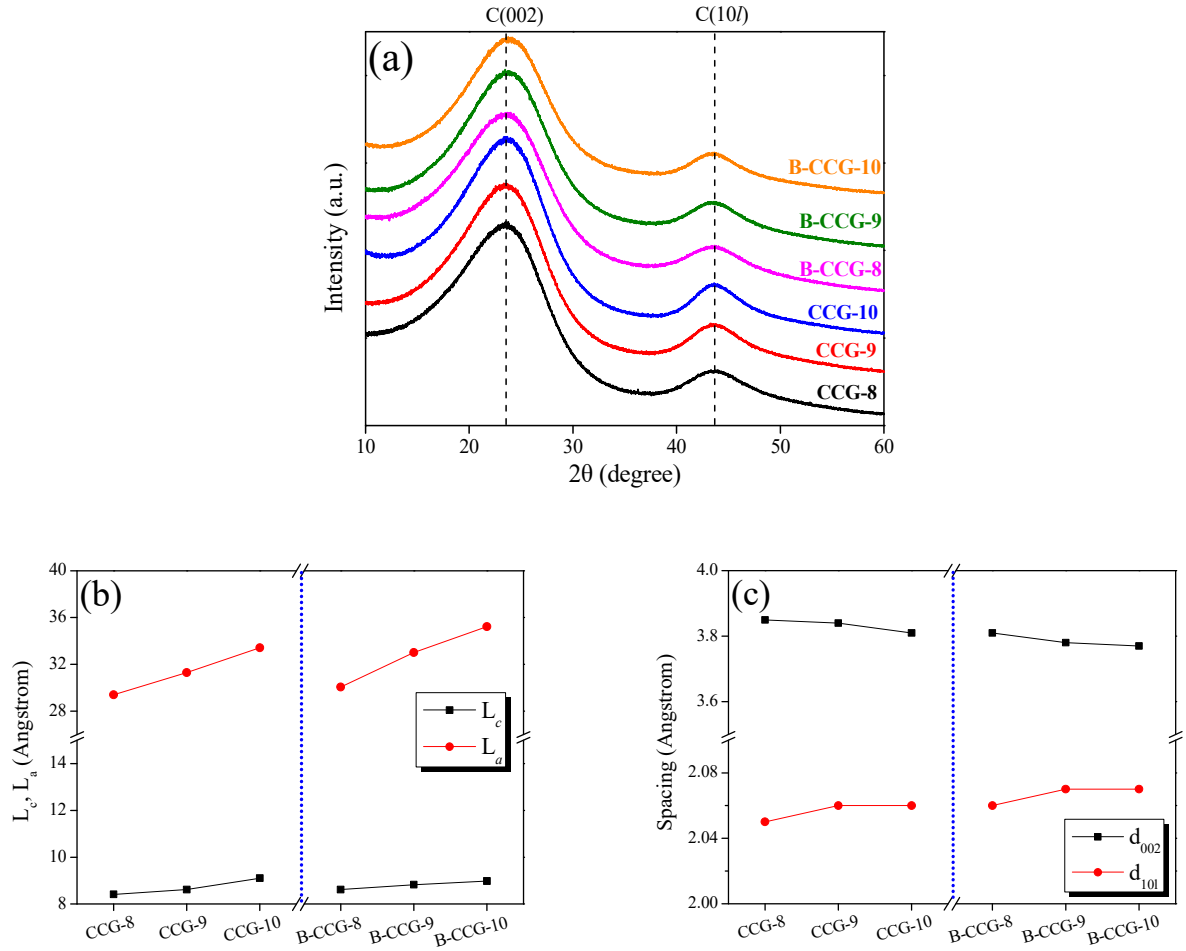

Figure 3. (**a**) X-ray diffraction patterns; (**b**) structural parameters; and (**c**) interplanar distances of PCG prepared with and without boric acid treatment as a function of carbonization temperature.

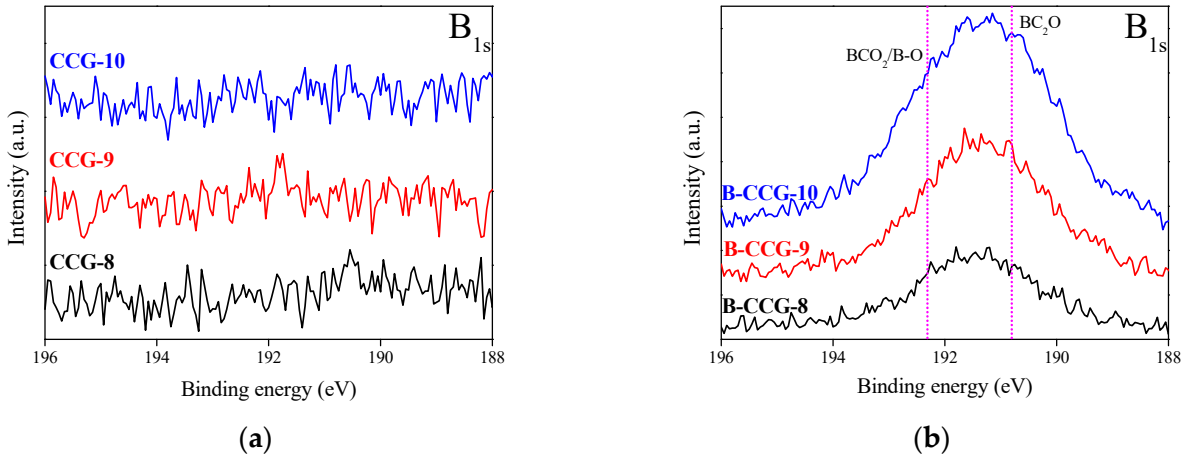

(**a**) (**b**)

Figure 4. B_{1s} spectra of CCG as a function of various carbonization temperatures with and without boric acid treatment; (**a**) CCG and (**b**) B-CCG.

Additionally, the C(002) peak of carbon materials appears near 26.5°, corresponding to the formation of a hexagonal honeycomb-like planar structure (2D) of carbon atoms via sp^2 hybridization. These planar carbon structures are stacked along the vertical direction, forming a three-dimensional structure where weak π–π interactions (Van der Waals forces) occur between the layers. The C(002) peak indicates the interlayer spacing of the vertically stacked planar structure, while the C(10*l*) peak represents the atomic arrangement of

carbon within the planar structure [48]. In other words, the (002) peak of carbon materials corresponds to the interlayer distance within the crystalline structure, while the (10*l*) peak indicates the interplanar crystalline spacing within the hierarchical structure.

Based on this, the increase in the L_a observed in Figure 3b and the decrease in d_{002} in Figure 3c can be attributed to grain growth in CCG and B-CCG as a result of increasing carbonization temperature. Notably, B-CCG exhibited a higher L_a value compared with CCG, which is likely due to the presence of boron introduced into the CCG. During the carbonization process, boron undergoes substitution reactions with carbon in CCG, forming functional groups such as B–C and B–O, thereby promoting enhanced grain growth in B-CCG. These findings are further corroborated by the XPS results of CCG and B-CCG presented in Figure 4.

Figure 4 shows the result of XPS analysis carried out to investigate the functional group bonding and surface characteristics of CCG following boron doping. The XPS survey spectra of the samples subjected to different carbonization temperatures and boric acid treatments are shown in Figure S3a, where C_{1s}, O_{1s}, and a small amount of N_{1s} peaks were identified in all samples. Due to the relatively low detection amount of the B_{1s} peak compared with other elements, high resolution spectral analysis was performed, as shown in Figure 4a,b.

The results indicate that while no B_{1s} peak was observed in CCG, clear detection of boron functional groups, including B–C and B–O bonds, was confirmed in B-CCG. Based on these findings, it can be inferred that boron atoms were successfully incorporated into the CCG structure by dry boric acid treatment. Notably, B-CCG-C10 exhibited the strongest B_{1s} peak, suggesting that boron doping was more effectively facilitated at higher carbonization temperatures. The chemical structure of the boron functional groups introduced into CCG is illustrated in Figure S4.

Figure 5 indicates the analysis of crystalline structure changes in PCG and B-PCG after activation treatment under the same experimental conditions as in Figure 3. As shown in Figure 5b, both the L_a and the L_c of PCG and B-PCG increase with increasing carbonization temperature, exhibiting a similar trend to that observed in Figure 3b. However, differences arise due to the distinct mechanisms governing crystallite growth during the carbonization and activation processes. While carbonization primarily promotes crystallite growth, the activation process induces pore development within the crystalline structure through oxidation reactions. As previously mentioned, the oxidation reaction of carbon materials preferentially occurs in amorphous carbon and at crystallite edges. Therefore, the observed increase in the L_a and the L_c of PCG and B-PCG can be attributed not only to crystallite growth at higher carbonization temperatures but also to the relative increase in crystallite proportion due to the oxidation of amorphous carbon and smaller crystallites during activation. Furthermore, a more pronounced increase in the L_a was observed in B-PCG compared with PCG, with B-PCG-C10 exhibiting the highest L_a value. Since boron can form both sp^2 and sp^3 hybridizations within the carbon structure, B-PCG is expected to undergo relatively disordered structure and exhibit a higher proportion of amorphous regions than PCG. This is supported by the lower L_a value and higher d_{002} observed for B-PCG-C8 compared with PCG-C8, as shown in Table S1 and Figure 4b. Additionally, the enhanced N_2 adsorption behavior of B-PCG in the $(P/P_0) < 0.01$ region of Figure 1 further confirms the relative increase in amorphous regions. During the carbonization process, boron incorporation influences the crystallite growth of CCG, leading to more significant grain development at higher carbonization temperatures (Figure 3b). In other words, B-CCG-C10 forms larger crystallites than other B-PCG samples and contains a relatively less amorphous region within the same volume. Therefore, the sharp increase in the L_a observed for B-PCG-C10 can be attributed to the preferential oxidation of amorphous regions during

activation, resulting in a relative increase in the proportion of crystallites. These results are further supported by the marked decrease in d_{002} of B-PCG with increasing carbonization temperature, as shown in Figure 5c.

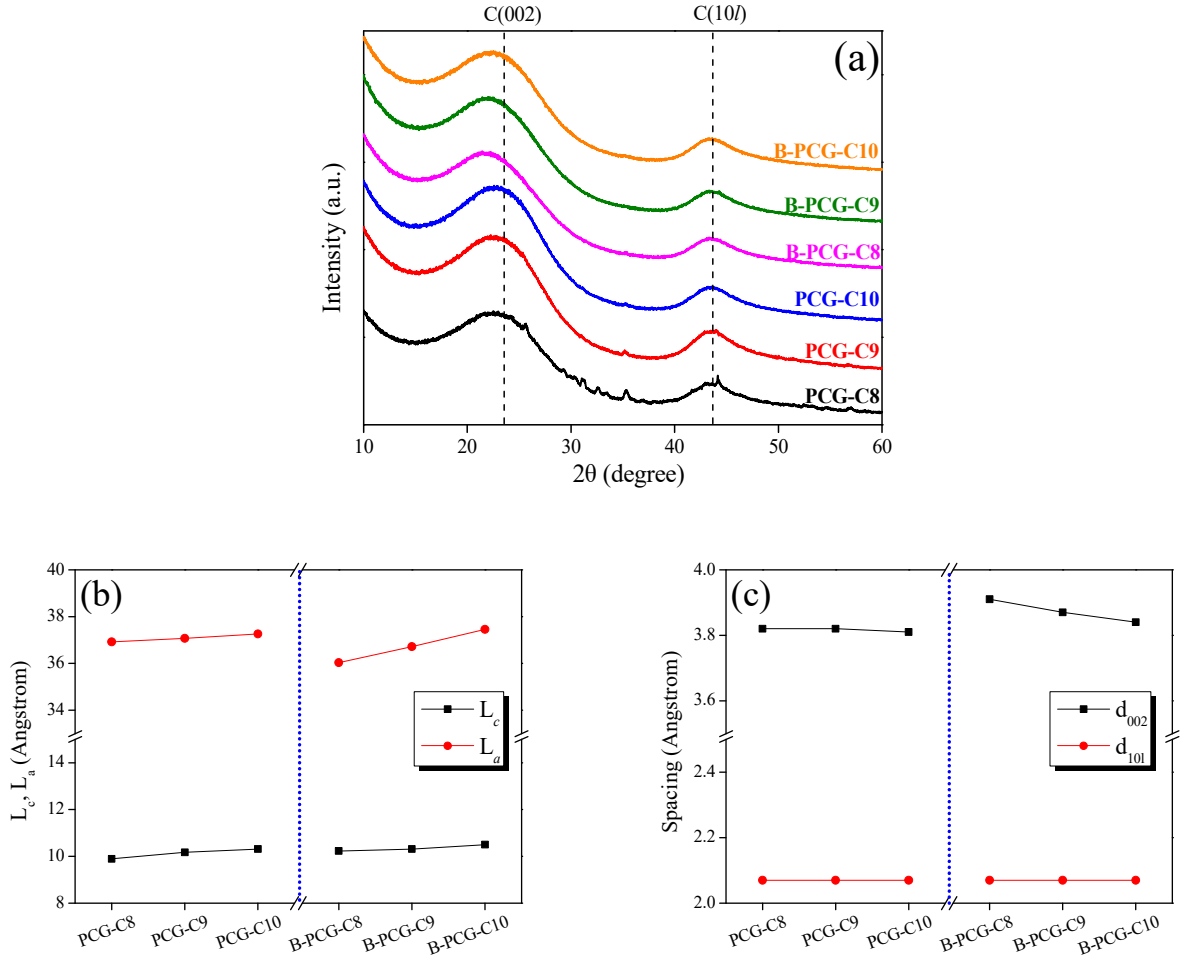

Figure 5. (**a**) X-ray diffraction patterns; (**b**) structural parameters; and (**c**) interplanar distances of PCG prepared with and without boric acid treatment as a function of activation temperature.

In Figure 5c, while the d_{002} value of PCG remains nearly constant with varying carbonization temperatures, B-PCG exhibits a significant decrease in d_{002}. This difference can be attributed not only to crystallite growth and the oxidation of amorphous regions but also to the influence of boron doping on the crystalline structure of PCG during activation. In particular, the oxidation reaction at the crystallite edges appears to be more pronounced in B-PCG compared with PCG. This is likely due to the presence of various boron functional groups (e.g., B–OH, B=O, B–C–O) at the crystallite edges, which facilitate oxidation reactions and induce structural changes during activation [49]. As the amorphous regions preferentially oxidize in this process, the alignment of the B-PCG crystalline structure improves, ultimately leading to a reduction in the d_{002} value.

Figure 6 shows the XPS analysis results of the surface functional group changes in PCG and B-PCG following activation treatment. The analysis confirmed the presence of boron functional groups exclusively in B-PCG. However, when compared with the results in Figure 4, a significant decrease in the intensity of boron functional groups was observed in B-PCG compared with B-CCG. This finding suggests that the boron functional groups bonded to the CCG surface acted as an "activation mediator" during the activation process. Mild boric acid treatment of the CCG surface by a dry method leads to the formation of various functional groups during carbonization (Figure 4b).

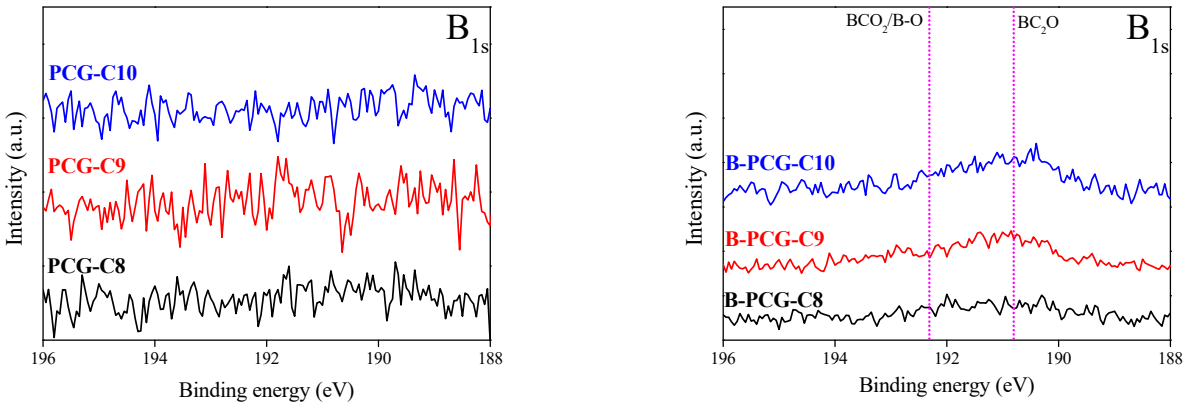

Figure 6. B_{1s} spectra of PCG as a function of various carbonization temperatures with and without boric acid treatment; (**a**) PCG and (**b**) B-PCG.

Since boron has a lower electronegativity than carbon, its incorporation into the carbon structure can modulate the electron density, thereby increasing the bonding energy. In particular, B–C sp^2 bonds enhance the thermal stability of B-CCG and contribute to the structural stability during the heat treatment process of carbonization. During the activation process, B-CCG undergoes partial oxidation of carbon, resulting in the formation of pores and its conversion into B-PCG. At this stage, boron present within the carbon structure can react with steam to form oxides such as B_2O_3. Since the resulting boron oxides have a high hydrophilicity, they readily react with steam during activation, subsequently transforming into intermediate oxides (B_xO_y), which volatilize and are eventually removed [50,51]. This pore development mechanism, facilitated by boron as an activation mediator, is supported by the increase in the specific surface area and mesopore formation in B-PCG with increasing carbonization temperature (Figure 1), as well as the reduction in boron functional groups (Figure 6b). As shown in Table 1, the proportion of mesopores in B-PCG gradually increases from 13.9% in B-PCG-C8 to 17.0% in B-PCG-C10. Thus, with increasing carbonization temperature, boron bonded to B-CCG not only promotes crystallite growth but also acts as an activation mediator to improve the overall pore characteristics during the activation process. Consequently, this mechanism can be described as a "hybrid activation" approach, in which chemically bonded boron facilitates pore development through a physical activation process. This approach demonstrates that it is possible to achieve a large specific surface area and well-developed porosity comparable to conventional chemical activation methods (Table S2).

3.3. Carbon Dioxide Capture Performance

Figure 7 presents the CO_2 adsorption isotherms of B-CCG and B-PCG measured at 0.5 bar. The CO_2 adsorption curves of undoped CCG and PCG are shown in Figure S5. In Figure 7a, the CO_2 adsorption capacity of B-CCG gradually decreases with increasing carbonization temperature. In contrast, as shown in Figure 7b (left), B-PCG exhibits approximately four times higher CO_2 adsorption capacity compared with B-CCG. This result suggests that boron doping facilitates the activation process of CCG by influencing the formation of micropores and mesopores in B-PCG (Figure 1 and Table 1). The resulting changes in pore structure increase the available physical adsorption sites for CO_2 molecules, ultimately contributing to an improved CO_2 storage capacity. Furthermore, the CO_2 adsorption capacity of PCG, shown in Figure S5b (left), is significantly lower than that of B-CCG. This phenomenon is attributed to the effect of boron doping, where boron-containing

functional groups such as B–CO, B–CO_2, and B–C_2O, identified in Figure 6b, function as a determining factor in enhancing the interactions with CO_2 molecules.

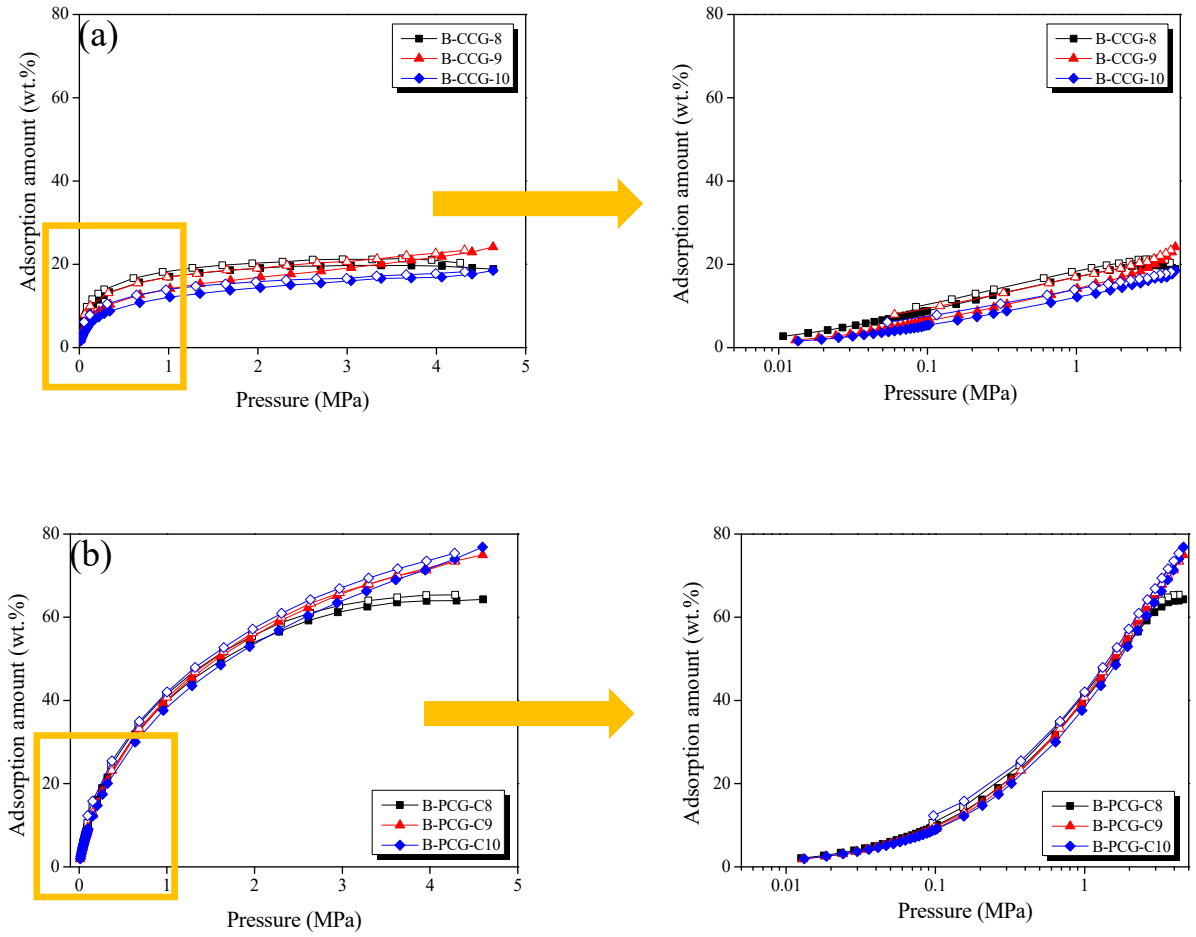

Figure 7. CO_2 storage capacity of boron-doped CGs under different heat treatment conditions as a function of carbonization temperature at 0.5 bar/298 K; (**a**) B-CCG and (**b**) B-PCG.

In particular, the B–CO_2 bond can facilitate the selective adsorption of CO_2 through Lewis acid–base interactions. This surface chemistry property enhances the CO_2 affinity of B-PCG, thereby positively influencing the CO_2 capture performance. This trend can be confirmed by comparing PCG in Figure S5b (left) with B-PCG in Figure 7b (left). Unlike PCG, for which CO_2 adsorption performance decreases with increasing carbonization temperature, B-PCG was observed to tend to increase CO_2 adsorption performance due to the presence of boron-containing functional groups on the surface. Therefore, boron doping plays a crucial role in modulating the surface chemistry and pore structure of carbon materials, ultimately improving their affinity for CO_2 molecules and enhancing CO_2 capture efficiency.

4. Conclusions

In this study, boron-doped porous carbon derived from coffee grounds (B-PCG) was synthesized using biomass waste as a precursor, and the effects of boron doping on the pore structure and surface chemical properties during carbonization and activation processes were systematically evaluated. During physical activation, boron functioned as an activation mediator to facilitate the development of porosity. Based on these findings, this study proposes a hybrid activation mechanism that utilizes the synergistic effects of chemical boron doping and physical activation. Compared with PCG, B-PCG exhibited significantly

enhanced specific surface area and pore development (Figure 1), which can be attributed to the thermal decomposition of boron-containing functional groups incorporated at the crystallite edges of PCG during carbonization. During activation, boron-doped carbonized carbon derived from coffee grounds (B-CCG) underwent oxidative reactions that resulted in the formation of hierarchical porosity and its subsequent conversion to B-PCG. At this step in the process, boron species present on the carbon surface reacted with steam to form boron oxides (e.g., B_2O_3), which acted as activation promoters. As a result, the specific surface area and mesopore formation increased, which correlated with the reduction of boron-containing functional groups, as confirmed in the XPS results (Figure 6).

The proposed hybrid activation mechanism was suggested in order to induce a level of porosity and surface area comparable to that achieved by conventional chemical activation. Consequently, B-PCG exhibited a 50% improvement in CO_2 adsorption capacity compared with PCG. This improvement is attributed to the increased interaction between boron functional groups and CO_2 molecules, as well as the development of mesopores that facilitate physical adsorption. Therefore, the hybrid activation-assisted boron doping represents a promising strategy for carbon capture and storage (CCS) applications.

Supplementary Materials: The following supporting information can be downloaded at: https://www.mdpi.com/article/10.3390/batteries11040158/s1, Figure S1: N_2/77K isothermal adsorption–desorption curves of B-CCG as a function of carbonization temperature; (a) normal and (b) logarithmic; Figure S2: Pore size distribution of B-CCG as a function of carbonization temperature; (a) calculated by BJH method, and (b) calculated by NLDFT method; Figure S3: XPS survey spectra of (a) CCGs and (b) PCG as a function of various processes conditions with and without boric acid treatment; Figure S4: Schematic of the boron doping process in CGs and the chemical structure of the introduced boron functional groups; Figure S5: CO_2 storage capacity of CGs as a function of various heat treatments at 0.5 bar/298 K; (a) CCG and (b) PCG; Table S1: Textural Properties of B-CCGs as a Function of Carbonization Temperature. Table S2. Specific surface area of porous carbon derived from waste coffee grounds as a function of the activation process. References [52–67] are cited in the supplementary materials.

Author Contributions: Conceptualization, H.H.K.; methodology, H.H.K.; software, H.H.K.; validation, H.H.K.; formal analysis, H.H.K.; investigation, H.H.K.; resources, K.-H.A. and B.-J.K.; data curation, H.H.K.; writing—original draft preparation, H.H.K.; writing—review and editing, H.H.K. and B.-J.K.; visualization, H.H.K.; supervision, B.-J.K.; project administration, K.-H.A. and B.-J.K.; funding acquisition, K.-H.A. All authors have read and agreed to the published version of the manuscript.

Funding: This research was funded by the "Carbon Industry Foundation project" no. 20016795 (Development of Manufacturing Technology Independence of Advanced Activated Carbons and Application for High-Performance Supercapacitor). In addition, this study was funded by the "Material Parts Technology Development Project" no. 20017563 (Development of Single-Walled Carbon Nanotube-Binder Integrated Conductive Material and its Application to High Energy-Density Secondary Battery Technology). This research was supported by the Jeonju University Research Year (K.H. An).

Data Availability Statement: The original contributions presented in the study are included in the article, further inquiries can be directed to the corresponding author.

Conflicts of Interest: The authors declare no conflicts of interest.

References

1. Dhillon, R.S.; Wuehlisch, G.V. Mitigation of global warming through renewable biomass. *Biomass Bioenerg.* **2013**, *48*, 75–89. [CrossRef]
2. Wienchol, P.; Szlek, A.; Ditaranto, M. Waste-to-energy technology integrated with carbon capture—Challenges and opportunities. *Energy* **2020**, *198*, 117352. [CrossRef]

3. Montagnini, F.; Nair, P.K.R. Carbon sequestration: An underexploited environmental benefit of agroforestry systems. *Agrofor. Syst.* **2004**, *61*, 281–295. [CrossRef]
4. Gill, L.; Bernardo, J. An approach to energy and climate issues aiming at carbon neutrality. *Renew. Energy Focus* **2020**, *33*, 37–42. [CrossRef]
5. Perissi, L.; Jones, A. Investigating european union decarbonization strategies: Evaluating the pathway to carbon neutrality by 2050. *Sustainability* **2022**, *48*, 4728. [CrossRef]
6. Paltsev, S.; Morris, J.; Kheshgi, H.; Herzog, H. Hard-to-abate sectors: The role of industrial carbon capture and storage (CCS) in emission mitigation. *Appl. Energy* **2021**, *300*, 117322. [CrossRef]
7. Shen, Y. Preparation of renewable porous carbons for CO_2 capture—A review. *Fuel Process. Technol.* **2022**, *236*, 107437. [CrossRef]
8. Makepa, D.C.; Chihobo, C.H. Sustainable pathways for biomass production and utilization in carbon capture and storage—A review. *Biomass Conv. Bioref.* **2024**, *16*, 1–22. [CrossRef]
9. Yin, Y.; Liu, Q.; Wang, J.; Zhao, Y. Recent insights in synthesis and energy storage applications of porous carbon derived from biomass waste: A review. *Int. J. Hydrogen Energy* **2022**, *47*, 39338–39363. [CrossRef]
10. Roussos, S.; de los Angeles Aquiáhuatl, M.; del Refugio Trejo-Hernández, M.; Gaime Perraud, I.; Favela, E.; Ramakrishna, M.; Raimbault, M.; Viniegra-González, G. Biotechnological Management Of Coffee Pulp—Isolation, Screening Characterization, Selection of Caffeine Degrading Fungi And Natural Microflora Present In Coffee Pulp And Husk. *Appl. Microbiol. Biotechnol.* **1995**, *42*, 756–762. [CrossRef]
11. Koul, B.; Yakoob, M.; Shah, M.P. Agricultural waste management strategies for environmental sustainability. *Environ. Res.* **2022**, *206*, 112285. [CrossRef]
12. Chakraborty, R.; Vilya, K.; Pradhan, M.; Nayak, A.K. Recent advancement of biomass-derived porous carbon based materials for energy and environmental remediation applications. *J. Mater. Chem. A* **2022**, *10*, 6965–7005. [CrossRef]
13. Jiang, T.; Zhang, Y.; Olayiwola, S.; Lau, C.; Fan, M.; Ng, K.; Tan, G. Biomass-derived porous carbons support in phase change materials for building energy efficiency: A review. *Mater. Today Energy* **2022**, *23*, 100905. [CrossRef]
14. Singh, Y.; Shdhu, H.S. Management of Cereal Crop Residues for Sustainable Rice-Wheat Production System in the Indo-Gangetic Plains of India. *Proc. Indian Natl. Sci. Acad.* **2014**, *80*, 95–114. [CrossRef]
15. Searchinger, T.; Heimlich, R.; Houghton, R.A.; Dong, F.; Elobid, A.; Fabiosa, J.; Tokgoz, S.; Hayes, D.; Yu, T.H. Use of US croplands for biofuels increases greenhouse gases through emissions from land-use change. *Science* **2008**, *319*, 1238–1240. [CrossRef]
16. Kaab, A.; Sharifi, M.; Mobli, H.; Nabavi-Pelesaraei, A.; Chau, K.W. Combined lifecycle assessment and artificial intelligence for prediction of output energy and environmental impacts of sugarcane production. *Sci. Total Environ.* **2019**, *664*, 1005–1019. [CrossRef] [PubMed]
17. Rivera, X.C.S.; Gallego-Schmid, A.; Najdanovic-Visak, V.; Azapagic, A. Life cycle environmental sustainability of valorization routes for spent coffee grounds: From waste to resource. *Resour. Conserv. Recycl.* **2020**, *157*, 104751. [CrossRef]
18. Liu, X.; Zhang, S.; Wen, X.; Chen, X.; Wen, Y.; Shi, X.; Mijowska, E. High yield conversion of biowaste coffee grounds into hierarchical porous carbon for superior capacitive energy storage. *Sci. Rep.* **2020**, *10*, 3518. [CrossRef]
19. Forcina, A.; Petrillo, A.; Travaglioni, M.; Chiara, S.; Felice, F. A comparative life cycle assessment of different spent coffee ground reuse strategies and a sensitivity analysis for verifying the environmental convenience based on the location of sites. *J. Clean. Prod.* **2023**, *385*, 135727. [CrossRef]
20. Bevilacqua, E.; Cruzat, V.; Singh, I.; Rose'Meyer, R.B.; Panchal, S.K.; Brown, L. The potential of spent coffee grounds in functional food development. *Nutrients* **2023**, *15*, 994. [CrossRef]
21. LeBouf, R.F.; Aldridge, M. Carbon monoxide emission rates from roasted whole bean and ground coffee. *J. Air Waste Manag. Assoc.* **2019**, *69*, 89–96. [CrossRef] [PubMed]
22. Cho, E.J.; Trinh, L.T.P.; Song, Y.; Lee, Y.G.; Bae, H.J. Bioconversion of biomass waste into high value chemicals. *Bioresour. Technol.* **2020**, *298*, 122386. [CrossRef] [PubMed]
23. Igliński, B.; Kujawski, W.; Kiełkowska, U. Pyrolysis of Waste Biomass: Technical and Process Achievements, and Future Development—A Review. *Energies* **2023**, *16*, 1829. [CrossRef]
24. Kalak, T. Potential Use of Industrial Biomass Waste as a Sustainable Energy Source in the Future. *Energies* **2023**, *16*, 1783. [CrossRef]
25. Tripathi, N.; Hills, C.D.; Singh, R.S.; Singh, J.S. Offsetting anthropogenic carbon emissions from biomass waste and mineralised carbon dioxide. *Sci. Rep.* **2020**, *10*, 958. [CrossRef]
26. Sri Shalini, S.; Palanivelu, K.; Ramachandran, A.; Raghavan, V. Biochar from biomass waste as a renewable carbon material for climate change mitigation in reducing greenhouse gas emissions—A review. *Biomass Conv. Bioref.* **2021**, *11*, 2247–2267. [CrossRef]
27. Kemp, K.C.; Baek, S.B.; Lee, W.G.; Meyyappan, M.; Kim, K.S. Activated carbon derived from waste coffee grounds for stable methane storage. *Nanotechnology* **2015**, *26*, 385602. [CrossRef]
28. Adan-Mas, A.; Alcaraz, L.; Arévalo-Cid, P.; López-Gómez, F.A.; Montemor, F. Coffee-derived activated carbon from second biowaste for supercapacitor applications. *Waste. Manag.* **2021**, *120*, 280–289. [CrossRef]

29. Chung, D.Y.; Son, Y.J.; Yoo, J.M.; Kang, J.S.; Ahn, C.Y.; Park, S.; Sung, Y.E. Coffee waste-derived hierarchical porous carbon as a highly active and durable electrocatalyst for electrochemical energy applications. *ACS Appl. Mater. Interfaces* **2017**, *9*, 41303–41313. [CrossRef]
30. Stylianou, M.; Agapiou, A.; Omirou, M.; Vyrides, I.; Ioannis, M.I.; Maratheftis, G.; Fasoula, D. Converting environmental risks to benefits by using spent coffee grounds (SCG) as a valuable resource. *Environ. Sci. Pollut. Res.* **2018**, *25*, 35776–35790. [CrossRef]
31. Kumari, R.; Singh, V.; Kant, C.R. Enhanced performance of activated carbon-based supercapacitor derived from waste soybean oil with coffee ground additives. *Mater. Chem. Phys.* **2023**, *305*, 127882. [CrossRef]
32. Kwak, H.S.; Kim, J.K.; Chun, Y. A review: Preparation and characterization of high-performance spent coffee grounds based adsorbent of for water treatment. *J. Korea Acad. Ind. Coop. Soc.* **2024**, *25*, 316–322. [CrossRef]
33. Hwang, J.; Kim, D. Development of Sustainable Packaging Materials Using Coffee Silverskin and Spent Coffee Grounds: A Comprehensive Review. *Korean J. Packag. Sci. Tech.* **2024**, *30*, 1–14. [CrossRef]
34. Ariharan, A.; Kim, S.K. Bioinspired sustainable Sheetlike porous carbon derived from Cassia fistula flower petal as an electrode for high-performance supercapacitors. *Energy Fuels* **2022**, *36*, 9337–9346. [CrossRef]
35. Ariharan, A.; Viswanathan, B. Porous activated carbon material derived from sustainable bio-resource of peanut shell for H2 and CO_2 storage applications. *Indian J. Chem. Technol.* **2018**, *25*, 140–149.
36. Chen, H.; Zhou, M.; Wang, Z.; Zhao, S.Y.; Guan, S.Y. Rich nitrogen-doped ord *Energy Fuels* ered mesoporous phenolic resin-based carbon for supercapacitors. *Electrochimica Acta* **2014**, *148*, 187–194. [CrossRef]
37. Wei, J.; Zhou, D.D.; Sun, Z.K.; Deng, Y.H.; Xia, Y.Y.; Zhao, D.Y. A controllable synthesis of rich nitrogen-doped ordered mesoporous carbon for CO_2 capture and supercapacitors. *Adv. Funct. Mater.* **2013**, *23*, 2322–2328. [CrossRef]
38. Ariharan, A.; Viswanathan, B.; Nandhakumar, V. Hydrogen storage on boron substituted carbon materials. *Int. J. Hydrogen Energy* **2016**, *41*, 3527–3536. [CrossRef]
39. Ariharan, A.; Viswanathan, B.; Nandhakumar, V. Heteroatom doped multi-layered graphene material for hydrogen storage application. *Graphene* **2016**, *5*, 39–50. [CrossRef]
40. Ariharan, A.; Viswanathan, B.; Nandhakumar, V. Nitrogen-incorporated carbon nanotube derived from polystyrene and polypyrrole as hydrogen storage material. *Int. J. Hydrogen Energy* **2018**, *43*, 5077–5088. [CrossRef]
41. Biscoe, J.; Warren, B.E. An X-Ray study on carbon black. *Int. J. Appl. Phys.* **1942**, *13*, 364–371. [CrossRef]
42. Urita, K.; Urita, C.; Fujita, K.; Horio, K.; Yoshida, M.; Moriguchi, I. The ideal porous structure of EDLC carbon electrodes with extremely high capacitance. *Nanaoscale* **2017**, *9*, 15643–15649. [CrossRef]
43. Lewandowski, W.M.; Ryms, M.; Kosakowski, W. Thermal Biomass Conversion: A Review. *Processes* **2020**, *8*, 516. [CrossRef]
44. Wang, Q.; Tian, D.; Hu, J.; Shen, F.; Yang, G.; Zhang, Y.; Deng, S.; Zhang, J.; Zeng, Y.; Hu, Y. Fates of hemicellulose, lignin and cellulose in concentrated phosphoric acid with hydrogen peroxide (PHP) pretreatment. *RSC Adv.* **2018**, *8*, 12714–12723. [CrossRef] [PubMed]
45. Sing, K.S.W. Reporting physisorption data for gas/solid systems with special reference to the determination of surface area and porosity. *Pure Appl. Chem.* **1985**, *57*, 603–619. [CrossRef]
46. Kim, J.H.; Kim, S.H.; Kim, B.J.; Lee, H.M. Effects of oxygen-containing functional groups on the electrochemical performance of activated carbon for EDLCs. *Nanomaterials* **2023**, *13*, 262. [CrossRef] [PubMed]
47. Kim, J.H.; Jung, S.C.; Lee, H.M.; Kim, B.J. Comparison of pore structures of cellulose-based activation carbon fibers and their applications for electrode materials. *Int. J. Mol. Sci.* **2023**, *23*, 3680. [CrossRef]
48. Kim, J.H.; Lee, H.M.; Jung, S.C.; Chung, D.C.; Kim, B.J. Bamboo-based mesoporous activated carbon for high-power-density electric double-layer capacitors. *Nanomaerials* **2021**, *1*, 2750. [CrossRef]
49. Enterría, M.; Pereira, M.F.R.; Martins, J.I.; Figueiredo, J.L. Hydrothermal functionalization of ordered mesoporous carbons: The effect of boron on supercapacitor performance. *Carbon* **2015**, *95*, 72–83. [CrossRef]
50. Kong, S.; Xiang, X.; Jin, B.; Guo, X.; Wang, H.; Zhang, G.; Huang, H.; Cheng, K. B, O and N codoped biomass-derived hierarchical porous carbon for high-performance electrochemical energy storage. *Nanomaterials* **2022**, *12*, 1720. [CrossRef]
51. Li, P.H.; Wu, W.J. Co-doping mechanism of biomass-derived nitrogen-boron porous carbon and its applications in energy storage and environmental purification. *J. Alloys Compd.* **2024**, *1002*, 175098. [CrossRef]
52. Wang, C.H.; Wen, W.C.; Hsu, H.C.; Yao, B.Y. High-capacitance KOH-activated nitrogen-containing porous carbon material from waste coffee grounds in supercapacitor. *Adv. Power Technol.* **2016**, *27*, 1387–1395. [CrossRef]
53. Poochai, C.; Srikhaow, A.; Lohitkarn, J.; Kongthong, T.; Tuantranont, S.; Tuantranont, S.; Primpray, V.; Maeboonruan, N.; Wisitsoraat, A.; Sriprachuabwong, C. Waste coffee grounds derived nanoporous carbon incorporated with carbon nanotubes composites for electrochemical double-layer capacitors in organic electrolyte. *J. Energy Storage* **2021**, *43*, 103169. [CrossRef]
54. Hadebe, L.; Cele, Z.; Gumbi, B. Properties of porous carbon electrode material derived from biomass of coffee waste grounds for capacitive deionization. *Mater. Today Proc.* **2022**, *56*, 2178–2183. [CrossRef]
55. Mengesha, D.N.; Abebe, M.W.; Appiah-Ntiamoah, R.; Kim, H. Ground coffee waste-derived carbon for adsorptive removal of caffeine: Effect of surface chemistry and porous structure. *Sci. Total Environ.* **2022**, *818*, 151669. [CrossRef]

56. Chiang, C.; Chen, J.; Lin, J. Preparation of pore-size tunable activated carbon derived from waste coffee grounds for high adsorption capacities of organic dyes. *J. Environ. Chem. Eng.* **2020**, *8*, 103929. [CrossRef]
57. Qian, M.; Xuan, X.Y.; Pan, L.K.; Gong, S.Q. Porous carbon electrodes from activated wasted coffee grounds for capacitive deionization. *Ionics* **2019**, *25*, 3443–3452. [CrossRef]
58. Liu, Y.; Lee, D.J.; Ahn, H.J.; Nam, S.Y.; Cho, K.K.; Ahn, J.H. Waste coffee grounds-derived carbon: Nanoarchitectured pore-structure regulation for sustainable room-temperature sodium–sulfur batteries. *Renew. Energy* **2013**, *212*, 856–874. [CrossRef]
59. Liu, S.H.; Huang, Y.Y. Valorization of coffee grounds to biochar-derived adsorbents for CO_2 adsorption. *J. Clean. Prod.* **2018**, *175*, 354–360. [CrossRef]
60. Park, M.H.; Yun, Y.S.; Cho, S.Y.; Kim, N.R.; Jin, H.J. Waste coffee grounds-derived nanoporous carbon nanosheets for supercapacitors. *Carbon Lett.* **2016**, *19*, 66–71. [CrossRef]
61. Pandey, K.; Jeong, H.K. Coffee waste-derived porous carbon based flexible supercapacitors. *Chem. Phys. Lett.* **2022**, *809*, 140173. [CrossRef]
62. Rufford, T.E.; Hulicova-jurcakova, D.; Zhu, Z.; Lu, G.Q. Nanoporous carbon electrode from waste coffee beans for high performance supercapacitors. *Electrochem. Commun.* **2008**, *10*, 1594–1597. [CrossRef]
63. Jutakridsada, P.; Prajaksud, C.; Kuboonya-Aruk, L.; Theerakulpisut, S.; Kamwilaisak, K. Adsorption characteristics of activated carbon prepared from spent ground coffee. *Clean. Technol. Environ.* **2016**, *18*, 639–645. [CrossRef]
64. Hung, Y.H.; Liu, T.Y.; Chen, H.Y. Renewable Coffee Waste-Derived Porous Carbons as Anode Materials for High-Performance Sustainable Microbial Fuel Cells. *ACS Sustainable Chem. Eng.* **2019**, *7*, 16991–16999. [CrossRef]
65. Hossain, R.; Nekouei, R.K.; Mansuri, I.; Sahajwalla, V. In-situ O/N-heteroatom enriched activated carbon by sustainable thermal transformation of waste coffee grounds for supercapacitor material. *J. Energy Storage* **2021**, *33*, 102113. [CrossRef]
66. Hsieh, T.H.; Wang, H.L.; Yu, G.T.; Huang, G.M.; Lin, J.H. Meso-pore dominant activated carbon from spent coffee grounds for high-performance electrochemical capacitors in organic electrolyte. *J. Environ. Chem. Eng.* **2021**, *9*, 106418. [CrossRef]
67. Kim, M.J.; Choi, S.W.; Kim, H.; Mun, S.; Lee, K.B. Simple synthesis of spent coffee ground-based microporous carbons using K_2CO_3 as an activation agent and their application to CO_2 capture. *Chem. Eng. J.* **2020**, *397*, 125404. [CrossRef]